ROLE OF GLACIERS IN HALTING SYRTIS MAJOR LAVA FLOWS TO PRESERVE AND DIVERT A FLUVIAL SYSTEM

A Thesis

Submitted to the Graduate Faculty of the
Louisiana State University and
Agricultural and Mechanical College
in partial fulfillment of the
requirements for the degree of
Master of Geology

in

The Department of Geology and Geophysics

by
Connor Michael Matherne
B.S., Louisiana State University, 2017
December 2019

ACKNOWLEDGMENTS

Special thanks to J.R. Skok and Jack Mustard for conceiving the initial ideas behind this project and to Suniti Karunatillake and J.R. Skok for their guidance. Additionally, thank you to my committee members Darrell Henry and Peter Doran for aid in understanding the complex volcanic and climate history for this location. This work has benefited from reviews and discussions with Tim Goudge, Steven Ruff, Jim Head, and Bethany Ehlmann. We thank Caleb Fassett for providing the CTX DEM processing of the outlet fan and Tim Goudge for providing the basin Depression CTX DEM. All data and observations used in this study are publically available from the NASA PDS. Derived products such as produced CTX DEMs can be attained through processing or contacting the primary author. Connor Matherne was supported by the Frank's Chair funds, W.L. Calvert Memorial Scholarship, NASA-EPSCoR funded LASpace Graduate Student Research Assistantship grant, and Louisiana Board of Regents Research Award Program grant LEQSF-EPS(2017)-RAP-22 awarded to Karunatillake. J.R. Skok was supported with the MDAP award NNX14AR93G. Suniti Karunatillake's work was supported by NASA-MDAP grant 80NSSC18K1375.

TABLE OF CONTENTS

ABSTRACT

The northeast edge of the Syrtis Major volcanic complex records a diverse history of volcanism and climate of early Mars. The region contains a stratigraphic record that spans the period of phyllosilicate secondary mineralogy from moderate pH alteration of the Early Noachian crust, to the more acidic, sulfate-forming, Hesperian period dominated by the adjacent volcanic plains of Syrtis Major Planum. A paleo-fluvial basin and channel system etched in the Syrtis Major volcanics is identified and analyzed using CTX and HiRISE imaging, CRISM observations and DEMs. These observations and analysis link the current landscape and the basin's existence at the base of the Syrtis Major lava flow to a paleo-glaciation within the Isidis Basin. This paleo-glaciation formed ice sheets kilometers thick and ranged over hundreds of kilometers laterally and is responsible for halting the Syrtis Major flows in the area to form the observed steep cliffs and the topographically flat mesa. Following this large scale glaciation, channels fed primarily by precipitation were etched into the Hesperian volcanics before filling the basin and flowing out an area of higher topography than is currently available due to the existence of an episodic ice dam before terminating in a potential, highly eroded, fan. The dynamic relationship between the climate and landscape evolution has left an imprint on the local geologic record of this complex region of Mars, with testable observations that could be made with the Mars 2020 Rover in the form of a highly jointed surface formed from lava ice interactions on the cliff face of the volcanic mesa.

1. INTRODUCTION

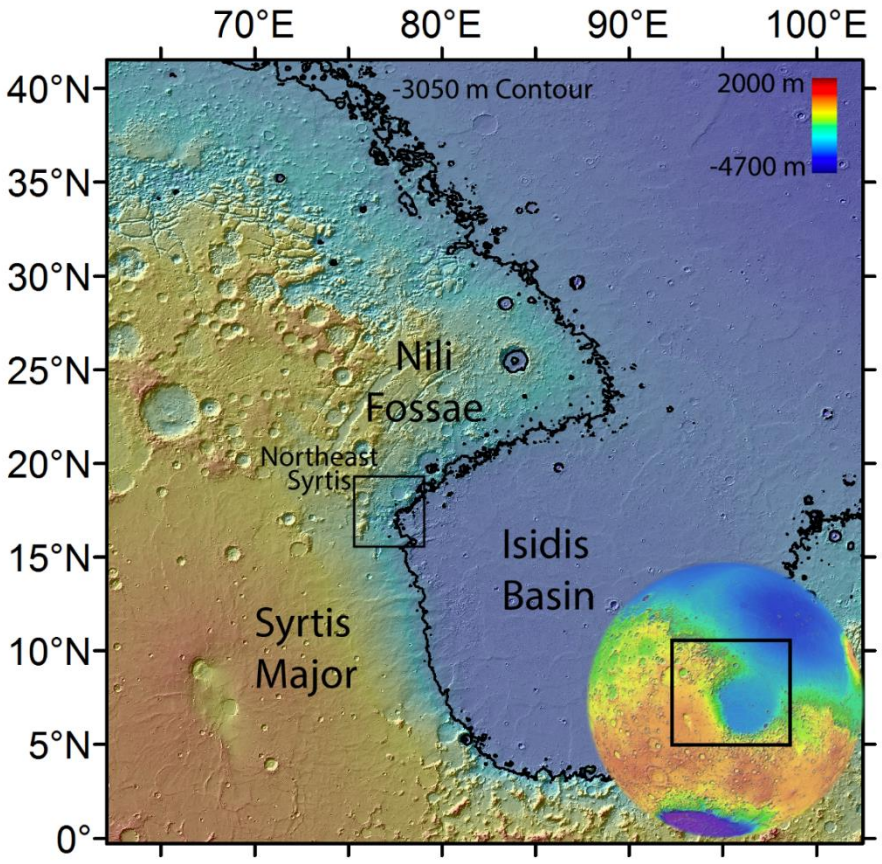

Figure 1. The regional context of Northeast Syrtis, with the Mars MOLA globe showing the location of the underlying image (box on globe).

The northeast edge of the Syrtis Major complex is located on the western edge of the Isidis Basin (Figure 1). The area contains a basin and channel system with many morphological features and geologic units that have been suggested to be related to a global ocean or regional ice sheet during the Hesperian (3 -3.7 Ga) (Bramble et al., 2017; Guidat et al., 2015; Quinn and Ehlmann, 2019). This northeast Syrtis Major area straddles the geologic boundary between the Noachian, clay-rich crustal exposures of Nili Fossae (Ehlmann et al., 2009; Mustard et al., 2009) and the Hesperian volcanics of Syrtis Major (Hiesinger and Head, 2004). The boundary is suggested to mark a global change in volcanic, fluvial and alteration activity (Bibring et al., 2006). The diversity of geologic processes and mineralogical units represented in the region makes it a complex but

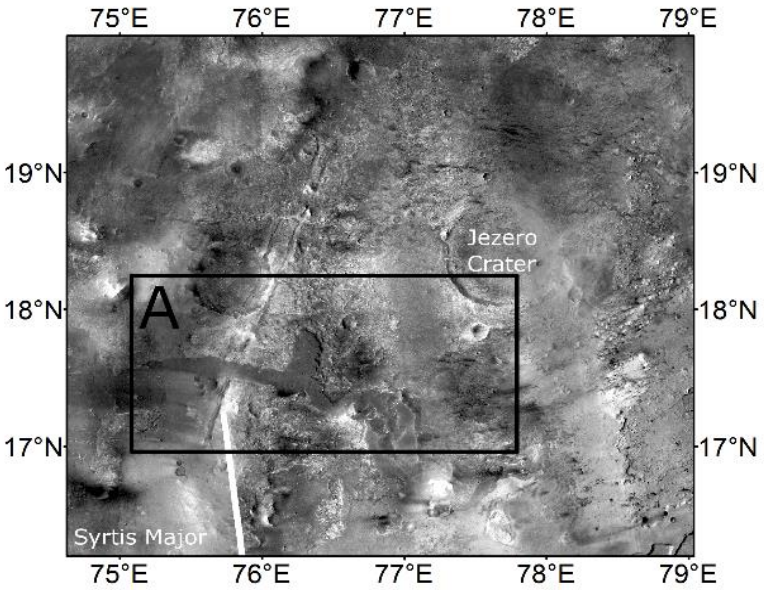

Figure 2. CTX mosaic of the study area contained within box A, bound to the north by Jerzero Crater, and to the south by Syrtis Major.

important region to understand. The oldest preserved local unit is the phyllosilicate-bearing Noachian (3.7 – 4.1 Ga) crustal bedrock that forms the modern plains to the north of Syrtis Major. The region was then shaped and excavated during the formation of the Isidis impact basin at ~3.96 ± 0.01 Ga (Werner, 2008) (Figure 2). The basin formation created the regional slopes and topography that influences later fluvial processes. Olivine-bearing [$(Mg,Fe)_2SiO_4$] units were then emplaced throughout the region stratigraphically above the altered bedrock. Emplacement of the olivine has been suggested as either impact melts from the Isidis event (Mustard et al., 2007), picritic lava flows (Tornabene et al., 2008), or more recent work suggesting the olivine is emplaced through detrital sedimentation due to their association with topographic lows (Palumbo and Head, 2018). This was followed by the tectonic formation of the Nili Fossae troughs (Wichman and Schultz, 2008) cross-cutting the olivine-bearing units (Mustard et al., 2009, 2007). The region was subsequently shaped by the impact that formed Jezero crater. Subsequent fluvial activity formed the Jezero crater lake (Figure 3) and deposited phyllosilicate-bearing deltas 3.74 Ga ago (Ehlmann

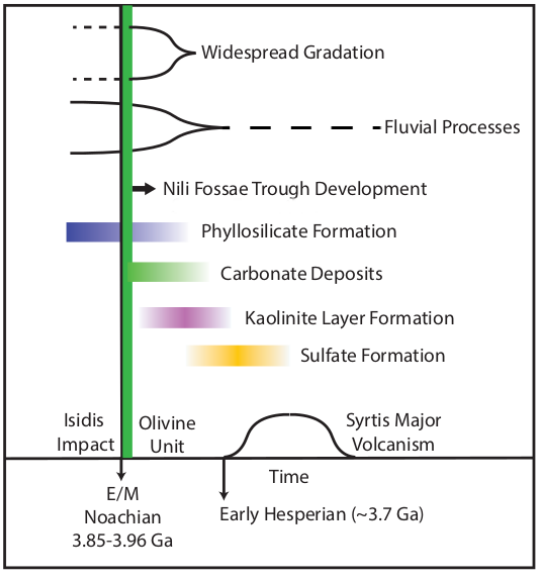

Figure 3. The proposed timeline of regional geology in Northeast Syrtis. (*Modified* from Mangold et al., 2008)

et al., 2008a; Fassett and Head, 2005; Goudge et al., 2015; Schon et al., 2012). The regional olivine-bearing unit was partially altered to a magnesium carbonate-bearing ($MgCO_3$) assemblage (Ehlmann et al., 2008b) and extensive surface leaching occurred in the altered phyllosilicate basement units to create zones of kaolinite [$Al_2Si_2O_5(OH)_4$]. Stratigraphically above those units is a sulfate-bearing layer capped by the low viscosity, basaltic Syrtis Major volcanic flows (Bandfield et al., 2000; Ehlmann and Mustard, 2012; Simpson et al., 1982). This sulfate unit has been suggested to be related to a global ocean or regional Isidis ice sheet (Souček et al., 2015) which would be required to explain the depositional history and further water loss fracturing and alteration of the unit (Quinn and Ehlmann, 2019).

The last major unit to be emplaced in the study region was the Syrtis Major volcanic lavas that cap the local stratigraphy to the immediate southwest of our study region (Hiesinger and Head, 2004; Schaber, 2008). The study of Syrtis Major's eastern cliff forming morphology and the knobby terrain transition from Syrtis Major to the Vastitas Borealis unit of the Northern Lowlands

suggests that the lavas may have encountered a volatile rich unit, such as an ice sheet (Edwards et al., 2013; Ivanov, 2003). Additionally, the lava flow margins are very irregular with steep cliffs indicating possible lava-ice interactions (Ivanov, 2003). The presence of ice deposits at mid-latitudes is predicted at times of high obliquity (Mustard et al., 2001) during the Amazonian (3 Ga to present) and may be more likely during an earlier, more volatile-rich period in Martian history with evidence for Hesperian aged glaciation at the Martian dichotomy, the contact between the Southern and Northern hemisphere, in other parts of Mars (Davila et al., 2013).

The geologic complexity of the transition and its surface visibility motivate our investigation to constrain the local, late stage fluvial history of Northeast Syrtis. The emplacement of the Syrtis volcanics was followed by a period of fluvial erosional activity as noted by Mangold et al., (2008), who described the presence of a channel etched elsewhere into the Syrtis basalts. That channel and several related nearby fluvial features would have required a significant source of water to create the observed channel morphology within the basalts, with 515 km^3 of water estimated to form the fracturing and expansiveness of the sulfates within the area (Quinn and Ehlmann, 2019). We expand on the work by Mangold et al., (2008) by investigating a set of Hesperian-aged geomorphologic features that are similar, but are instead located on the transition from the Hesperian volcanics to the adjacent Noachian terrains. We complement prior works by Bramble et al., (2017) who characterized the morphology of the geologic units, and several others who have provided spectral analysis (Ehlmann et al., 2008b; Goudge et al., 2015; Mustard et al., 2009), by focusing our analysis on the shallow dipping sedimentological surface units within the basin, such as a magnesium carbonate layer and sulfate units tracing the topography contours within the basin.

In this paper, we respond to three preliminary questions motivated by the basinal landscape. Question 1: what are the likeliest hydrological sources for the upland source channels? Question 2: what terminated a large volcanic flow to preserve an isolated basin? Questions 3: what enabled basin drainage via topographically higher outlet channels, despite the existence of a topographically lower potential outlet to the SE? With these three questions addressed, we look to answer an overarching question that encompasses all of our previous results: to what extent do the findings suggest glacial activity at this geologic transition zone?

1.1. Local Fluvial System Features

The Northeast Syrtis region's fluvial morphology can be placed into two main periods. The first period is characterized by the paleo-meandering rivers (Schon et al., 2012) and the delta formation in the Jezero Crater open basin lake (Ehlmann et al., 2008a; Fassett and Head, 2005), dated at 3.74 Ga (Fassett and Head, 2008). This period pre-dates the Hesperian-aged volcanics that embay the lacustrine deposits (Goudge et al., 2012). The second period post-dates the Hesperian volcanics of Syrtis Major, with sources within the volcanic terrains as we explore here. Given these two episodes of fluvial processes, we subdivide the region of interest into upland source channels, basin, outlet channel, and channel fan (Figure 4). Current literature has mentioned the existence of the upland source channels (Hiesinger and Head, 2004), the basin (Bramble et al., 2017), and the outlet channels (Quinn and Ehlmann, 2019), however, the channel termination remains unaddressed in the literature.

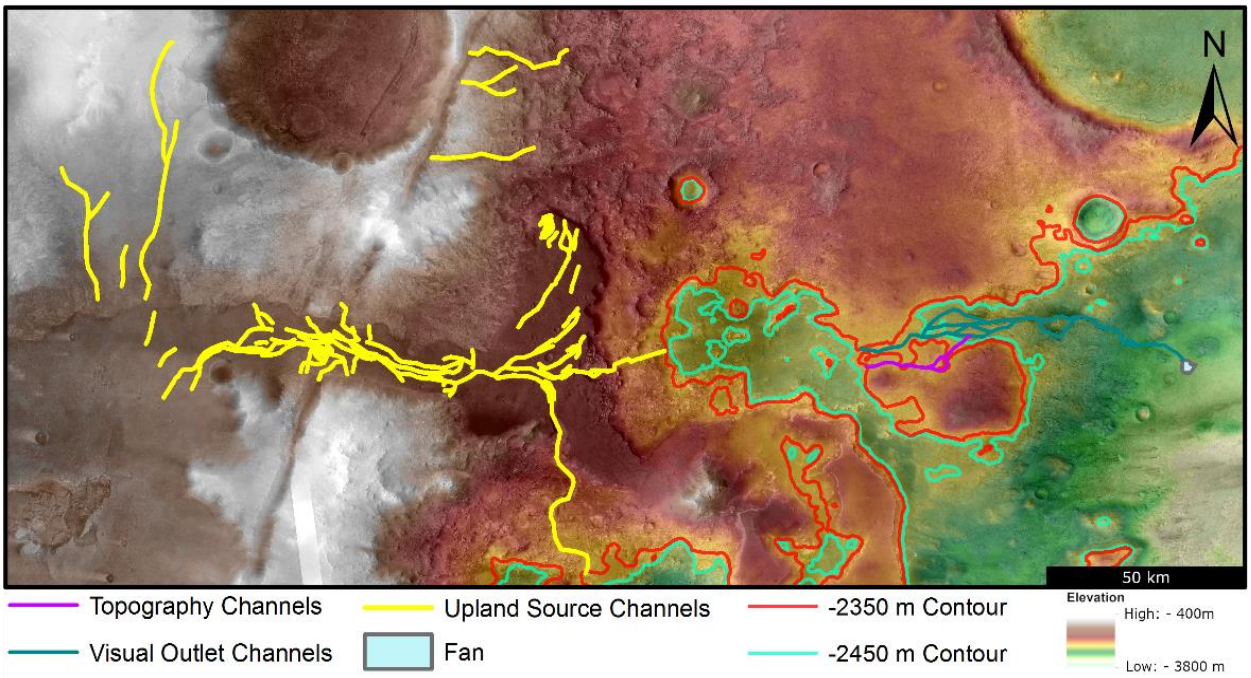

Figure 4. Context Camera (CTX) mosaic, with colored High Resolution Stereo Camera (HRSC) Digital Elevation Model (DEM) overlay of the channel system on the edge of Northeast Syrtis.

1.1.1. Upland Source Channels

A morphologically subdued system of upland channels is apparent on top of a broad lava flow emplaced in the early Hesperian (Hiesinger and Head, 2004) (Figure 5). The braided, shallow channels start in the west and follow a shallowly dipping, 7 km wide basaltic lava flow that previously floored a topographic low in the Noachian-aged material (Figure 5A). In extending beyond the basaltic unit, the channels cross a flat-topped volcanic mesa that is a few kilometer long (Figure 5B) with cliffs over 100 m in height (Figure 5E). On the mesa, the channels spread

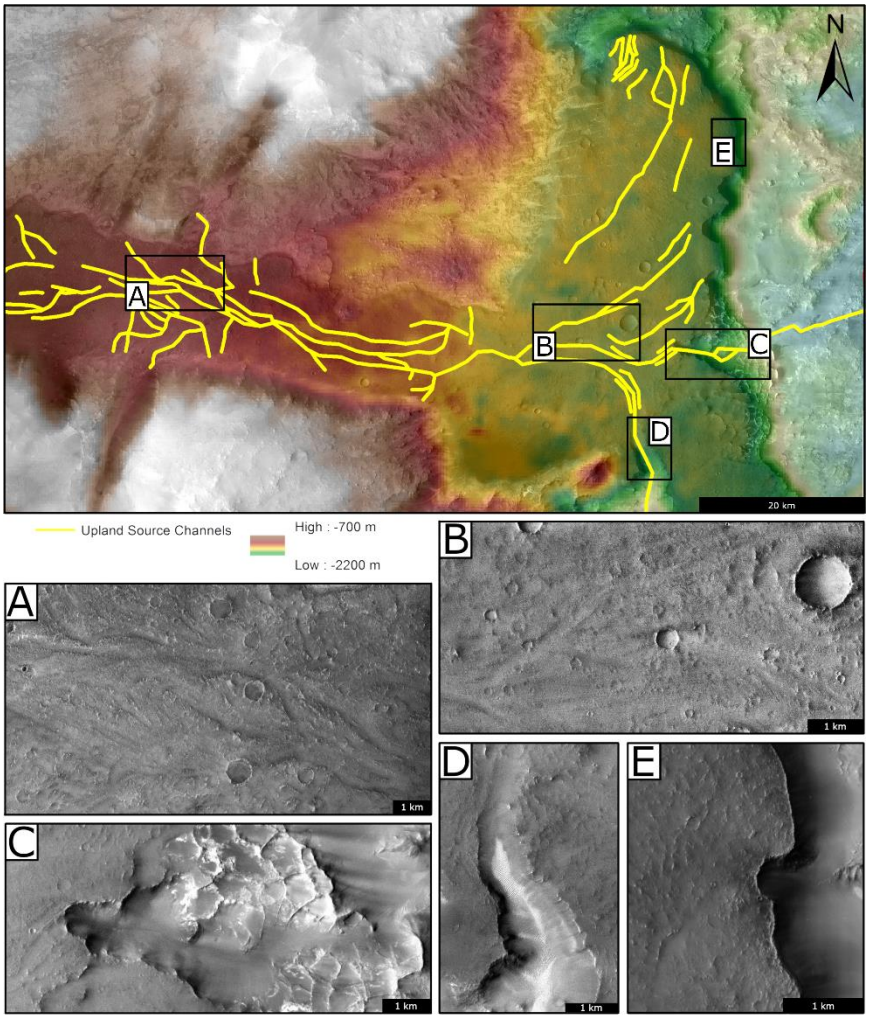

Figure 5. Upland source channel terrain. A) Braided erosional grooves. B) Flow features that eroded the igneous rock layer along the topographically flat volcanic mesa. C) Light-toned sulfate bearing material near basin inlet channel. D) Southern channel eroding into the Syrtis Major volcanics E) Highly irregular boundary of the volcanic flows with steep cliffs over 100 m high.

predominantly to the east and the south, along with several minor extensions in different directions. The southern channel (Figure 5D) leads to a closed basin immediately south of this plateau. The eastern channel system (Figure 5C) continues off the volcanic plateau and erodes a channel that leads to the basin.

1.1.2. Basin

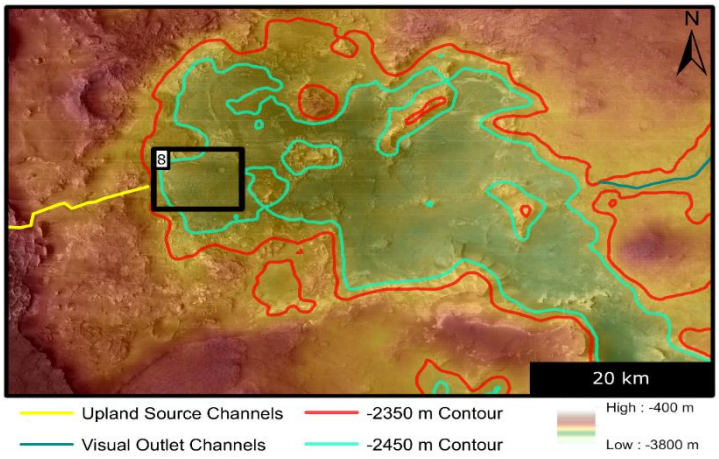

Figure 6. CTX mosaic with colored HRSC DEM overlay shows a topographic low that forms the basin of the purported past fluvial system. Black box shows location of Figure 8.

The eastern channel mentioned above leads directly to a topographic basin centered at 17.6°N 76.6°E (Figure 6). The basin depression is ellipsoidal with an elongate southeast-northwest axis. The basin contains two potential outlet paths, one to the east, and one to the southeast. The southeast outlet is floored by loose material that has been derived from adjacent cliff forming volcanics (Bramble et al., 2017). A lake would be required to have filled this basin in order to activate these outlet channels (Quinn and Ehlmann, 2019).

1.1.3. Outlet Channels and Termination

The basin has an outlet channel system on its eastern edge, with no outlet channels observed in the southeastern passage (Quinn and Ehlmann, 2019). The outlet channel erodes through the friable Noachian terrain for 48 km before terminating at an elevation of -3050 m at the edge of the Isidis Basin (Figure 7).

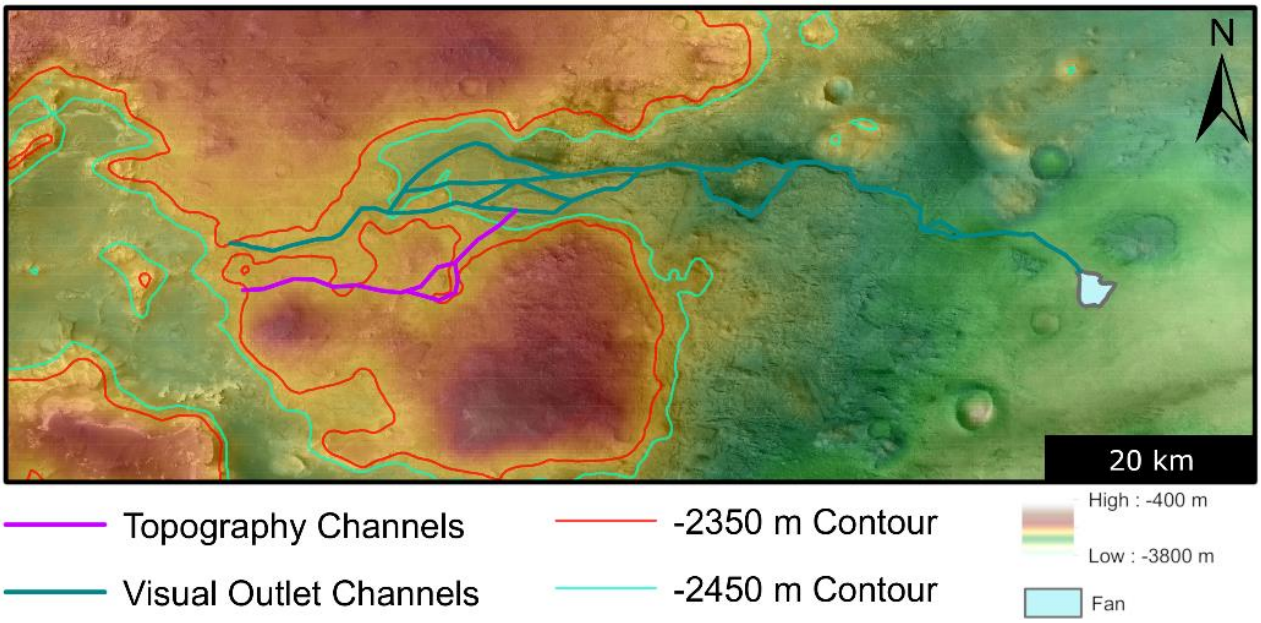

Figure 7. Mapped outlet channels. Topography shows multiple eroded channels flowing from west to east before terminating in a fan. Four visually distinct and two additional potential channels derived from topography could have been active during different fluvial episodes as evident in the DEM overlay

2. METHODS

Surface morphology was assessed using ~6 m/pixel images from the Context Camera (CTX) instrument on the Mars Reconnaissance Orbiter (MRO) (Malin et al., 2007). Detailed morphology was also investigated using ~0.25 m/pixel images from the High Resolution Imaging Science Experiment (HiRISE) instrument on MRO (McEwen et al., 2007) where available. All imaging data is maintained in an ArcMap GIS database (Table 1). Topographic information and regional slope were determined using transects with Mars Orbiter Laser Altimeter (MOLA) gridded topography with a resolution of 128 pixels per degree (Zuber, 1992), and High Resolution Stereo Camera (HRSC) (Neukum and Jaumann, 2004) Digital Elevation Models (DEM). Local topography has been determined with CTX derived DEM. CTX DEMs were produced with the NASA Ames Stereo Pipeline software (Edwards and Broxton, 2012) or provided by the USGS Astrogeology Science Center using a blend of MOLA and HRSC images allowing for vertical accuracy as fine as 10 m (Fergason et al., 2018). A normalized and seamless mosaic was provided for the area by the Bruce Murray Laboratory for Planetary Visualization (Dickson et al., 2018). Channel branching angle is determined using CTX and HiRISE images by dividing up the channels into stream segments and finding the junction angle between these two segments (Seybold et al., 2017).

Mineral composition was determined with reflectance spectra by the Compact Reconnaissance Imaging Spectrometer for Mars (CRISM), a visible and near-infrared (VNIR) hyperspectral imaging instrument (Murchie et al., 2007). CRISM acquires full resolution targeted (FRT) images at 18 meter per pixel spatial resolution and 544 spectral bands ranging from 0.36 – 3.9 μm (Murchie et al., 2007). CRISM images were calibrated with a volcano scan method (McGuire et al., 2009) to eliminate atmospheric effects and ratioed against spectrally bland areas

covered by dust of average albedo and illumination within the image to improve detection of minerals with absorption bands that lie within spectral bands ranging from 1.9 – 2.1 μm. The spectrum were compared against a library of laboratory spectrum within the Crism Analysis Toolkit. Table 1 lists examples of image and spectral data that we used.

Ages of the volcanic capping units were determined using CraterStats 2 within ArcMap using CTX images for the Syrtis Major volcanic unit to the west and two capping units within the basin (Figure 10). Other areas within and around the basin were not counted due to low crater retention, stemming from friability which is up to 78% lower than the volcanic units chosen (Palumbo and Head, 2018). We followed the guideline of at least three orders of magnitude larger area than the smallest diameters for the craters, while maintaining crater diameters to be larger than 100 m to avoid large uncertainties (Hartmann, 2005). No secondary craters were observed within our units, a major critique of the crater counting method when using smaller craters as noted by McEwen et al., (2005).

3. RESULTS

3.1. Upland Source Channels

The braided upland source channels etch the volcanic landscape with a diffuse origin and no clear origin. The channels bifurcate at twenty different locations at an average angle of 43° ± 21° as they move down the volcanic slope before dispersing into multiple paths on the volcanic mesa. The channels exit the mesa by diverting to two different areas: one into the basin to the east, the other off the mesa to the south. The major system that is directed south erodes back the mesa 4.2 km (Figure 5D), and ends in a potential terminal fan roughly 20 km from the mesa. The other system trends eastward off of the mesa, eroding it back a distance of 3.5 km (Figure 5C). The channel continues easterly as it encounters a boxwork texture of light-toned sulfate bearing material (Quinn and Ehlmann, 2019) before entering the basin (Figure 5C).

3.2. Basin

Current topography shows that the basin would drain via a 3 km wide gap to the southeast if filled above the -2450 m, 100 m lower than the water height that would have activated the outlet channel to the east (Figure 6). However, we find no major indications of fluvial morphology or modification to suggest runoff in the southeastern gap. While this gap is floored by loose material that may obscure any of these features, we do not observe any of these features emerging once the loose material has lessened. When discharge was occurring only through the northeastern outlet channel, the lake would cover approximately 300 km^2 with a maximum depth of 200 m. Along the

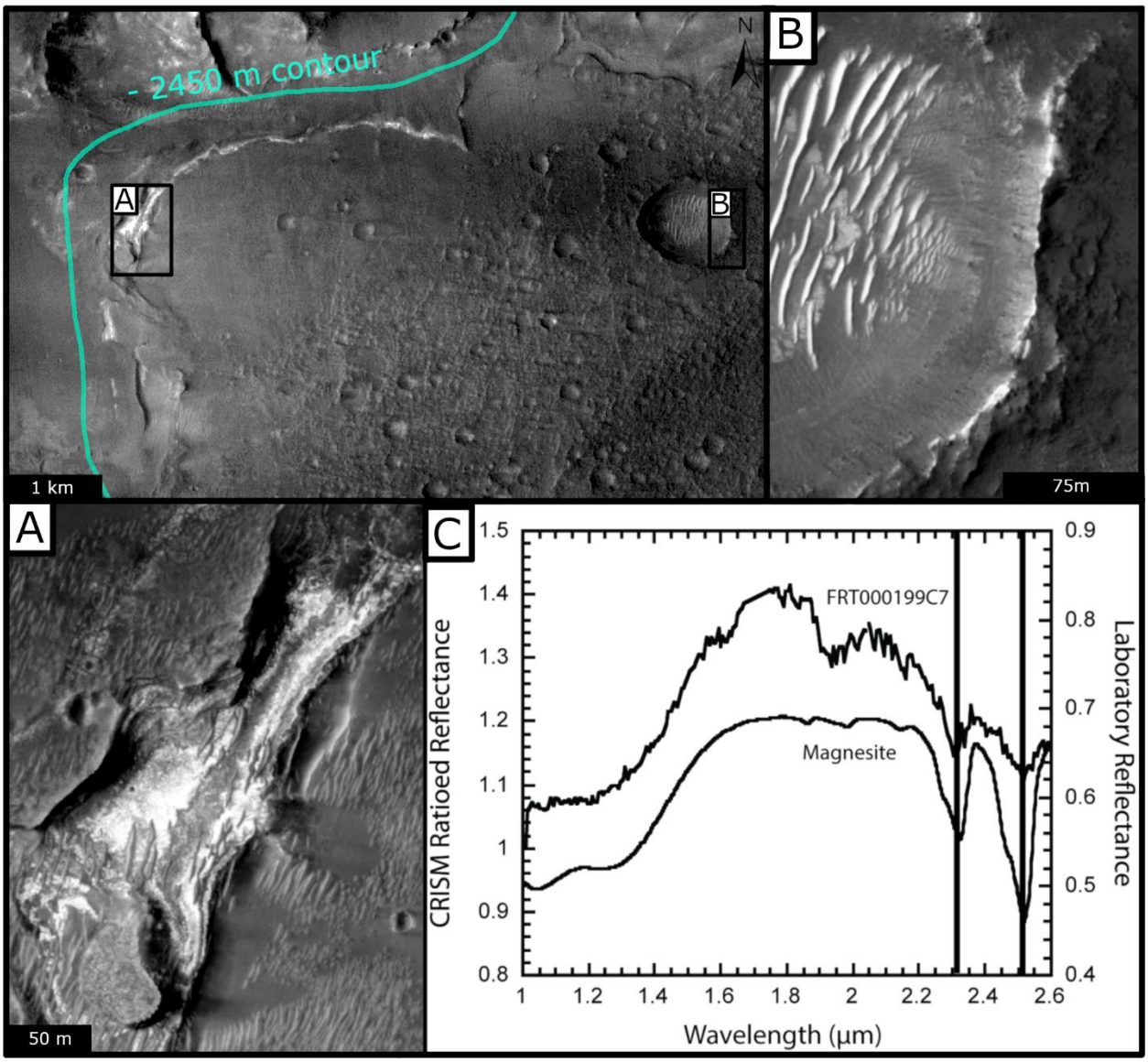

Figure 8. CTX view of basin fill unit. A) The fill unit is surrounded by light-toned, layered olivine and magnesium carbonate deposits that trace the topography. B) Carbonates underlying the fill unit and exposed around the edges of a 500 m crater. C) CRISM of magnesium carbonate ($MgCO_3$) on edge of basin fill units. (FRT000199C7) Laboratory magnesite spectra for comparison (RELAB: LACB03B). Characteristic absorption features marked for magnesium carbonate (Ehlmann et al., 2008b).

eastern side of the basin, light-toned, spectrally-dominated magnesium carbonate layer based on CRISM observations can be seen tracing the topography in the area and is exposed in the rims of nearby impacts (Figure 8).

3.3. Outlet Channels

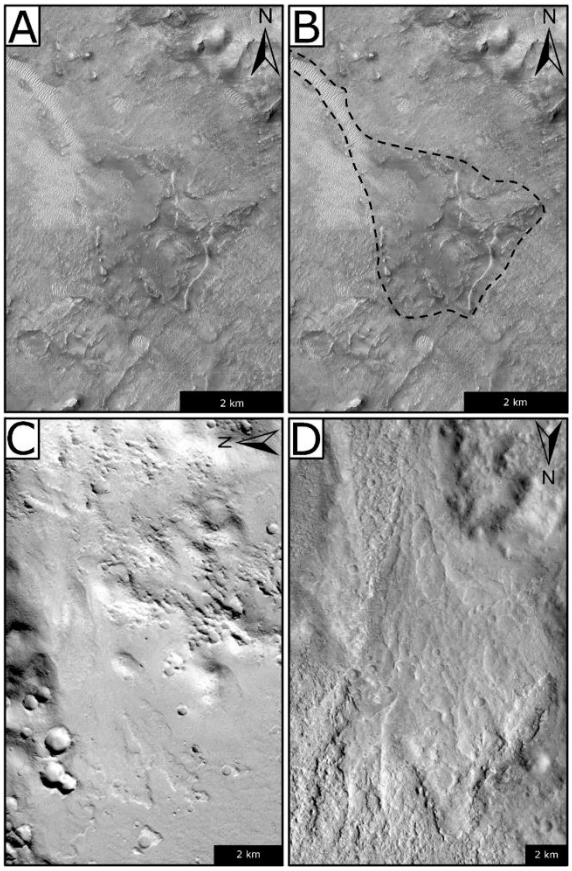

Figure 9: A) The outlet channel leads to a deeply eroded, 2.1 km^2 fan. B) Fan and channel outlined in a black dashed line for ease of identification. C) Highly eroded fan located within Sagan Crater (Salese et al., 2019) D) Highly eroded delta located in Libya Montes (Erkeling et al., 2012).

The proposed lake inside the basin would have emptied through an outlet channel that drained east, carving through the Noachian phyllosilicate-bearing crust (Figure 7). This channel can be traced for 48 km as it drops ~750 m from an elevation of -2330 m at the basin rim to -3050 m elevation eastward. The channel begins with a well-defined ~500 m wide path. After the first ~7 km, the channel morphology becomes complex with signs of braiding or multiple channel forming episodes. One section, 10 to 25 km from the head, contains a branching path that contains at least four distinct sub-channels. The channel also bifurcates 30 to 35 km from the head. In

addition, from the start at the basin, there are two potential topographic channels. Using the combined visual and topographic mapping, we can identify at least six variations in the outlet path. Sections of the channel are subdued, but a majority are well defined with sharp sides. Much of the length of the channel floor now has aeolian ripples that are consistently perpendicular to the channel walls before terminating.

3.4. Outlet Channel Termination

The channel terminates at -3050 m and forms a heavily dissected fan (Figure 9) that covers an area of 2.1 km^2. The fan does not show significant topography at the resolution of a CTX DEM (10 m vertical) beyond the regional slope. About 12.5 km downslope from the fan, two additional channel fragments, 4 km in length and morphologically similar to the outlet channel (in terms of width, depth, and sinuosity), are separated by basin floor material. Due to the friability of the local geology and the size of the fan, we are unable to determine the fan age using crater counting methods.

3.5. Dating of the Volcanic Units

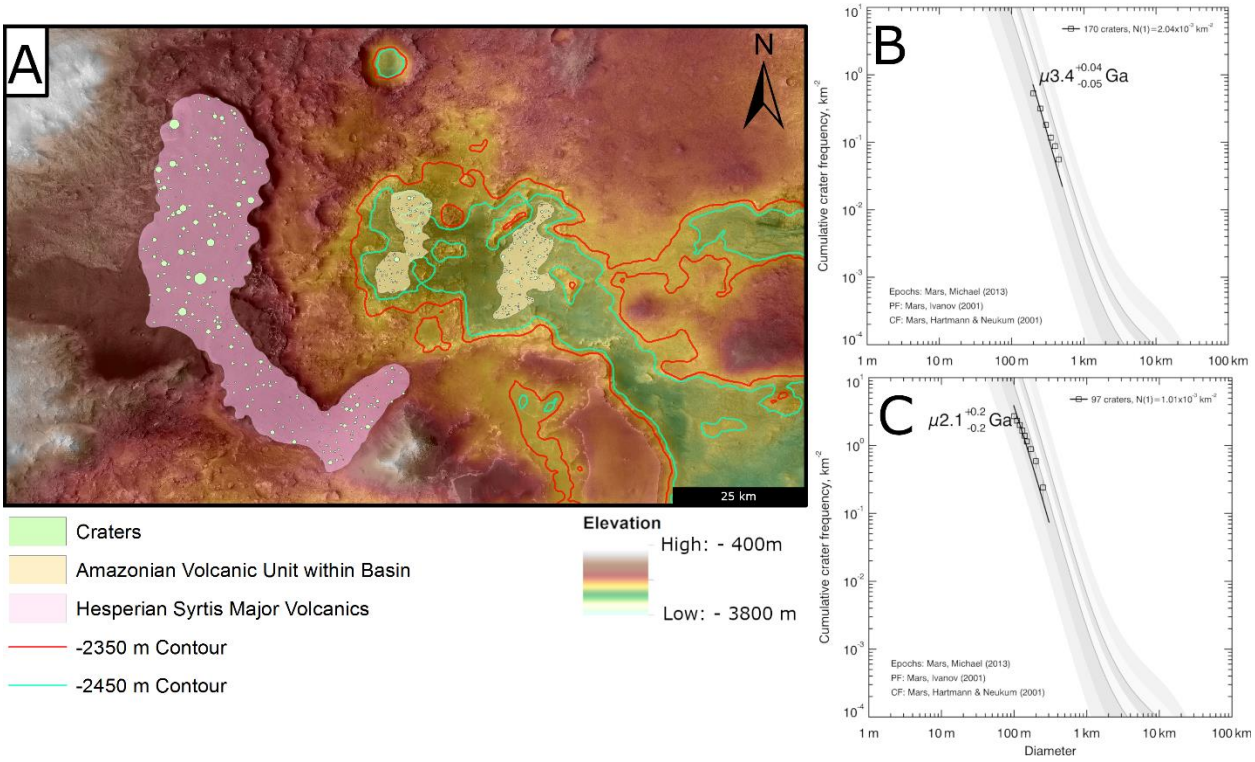

Figure 10. A) CTX mosaic shows the three regions which were crater counted. Two areas within the basin were dated to the Amazonian (C) while the larger unit to the west is dated to the Hesperian (B). Plots for both B and C were created using Craterstats 2.0 (Hartmann, 2005).

The Hesperian Syrtis Major Volcanics were crater counted to an age of 3.4 ± 0.05 Ga using 170 craters within the area (Figure 10B). The Amazonian Volcanic Unit within the basin was dated to 2.1 ± 0.2 Ga for the eastern unit using 97 craters (Figure 10C). The western unit within the basin was dated to the same age of 2.1 ± 0.2 Ga using 99 craters.

3.6. Estimations for Syrtis Major Volcanic Flow Thickness

Two major characteristics of the Syrtis Major volcanic flows of interest are the critical thickness, the thickness at which the lava will no longer flow, and the height of the cliffs that these flows formed. The critical thickness is calculated using the equation:

$$h = \frac{S_y}{g\rho \tan\alpha}$$

where S_y is lava yield strength, g is gravity, ρ is density and α is the angle of the slope (Rothery et al., 2003). In order to get a range of probable critical thicknesses, we use a value of 3.72 m/s^2 for g (Hirt et al., 2012), ρ of 3000 kg/m^3 assuming standard basaltic composition (Stolper and Walker, 1980), and a regional slope of 12°. We vary the lava yield strength parameter in order to give us the widest range of possible thickness by using low end from Mauna Loa, Hawaii of 3.5×10^2 Pa, and high end from Ascraeus Mons of 8.3×10^4 (Wilson and Head, 1994). This returns values of .15 m and 3.5 m respectively for the critical thickness. The cliffs on the volcanic mesa are consistently over 100 m in height, with the northeastern side containing the largest cliffs at over 200 m high.

4. DISCUSSION

Having described each of the components of this basin system separately, we now integrate the observations to interpret the underlying geologic processes. We will assess each question, its importance, and offer potential hypotheses to explain the observations before addressing their significance to glacial activity.

4.1. Question 1. What are the likeliest hydrological sources for the upland source channels?

In addressing Question 1, we observe in Figure 5A that the channels bifurcate and etch through the volcanic cap rock until they erode back the edge of the volcanic plateau (Figure 5D, E). Of those, only the most eastwardly channel connects to the basin via surface morphology while the others travel to parts of the surrounding terrain, with laterally fading geomorphic expression. Those upland channels have no clear point origin. While a fluvial origin has been favored, we have considered alternative mechanisms, including effusive lava channels. However, the lack of a spatially localized source, the meanders, lack of a debris field, and the erosion at the edge of the plateau are collectively more consistent with fluvial erosion rather than a lava channel formation (Crown and Ramsey, 2017; Susko et al., 2017).

Groundwater sapping was also considered as a source of the channels given the existence of other groundwater systems south of this area (Mangold et al., 2008). However, this area is topographically higher by over 1 km than estimated groundwater depth during the Hesperian. More recent research has shown that water can be transported through pressure gradients upwards to the surface through confinement within dikes to an elevation of roughly -4000 m at this latitude (Salese et al., 2019). Extensive dike formations associated with both Syrtis Major and the Isidis Basin could possibly displace the groundwater table this way. However, we do not see morphology

consistent with groundwater sapping, such as fissures, or stepped deltas. In addition, the dike-controlled water table would require elevation differences for sapping far greater than what has been observed in previous studies (Salese et al., 2019). Other suggested sources include subsurface outflows from aquifer over-pressurization, possibly from volcanic heating, impact fracturing of overlaying units, or the raising of subsurface water tables (Andrews-Hanna et al., 2007). However, such point sources are not observed in our study region.

In contrast to alternatives, the lack of a localized origin for these channels can indicate a distributed source for fluvial activity. Precipitation in the form of snow or ice, with subsequent basal melting of ice deposits would leave no erosional marks until the runoff concentrated to the point of carving the observed channels. Mangold et al., (2008) described several potential sources for the channels observed to the south of our study region. Alternatively, periodic high obliquity (Laskar et al., 2004) may enable low latitude ice deposits in the region. Basal melting of such ice could provide the fluids required to carve the observed morphology and could focus the flow along specific channels. A widespread surface ice source would explain the diffuse nature of the source fluvial morphology on the volcanic rocks and the lack of a localized source, similar to that we see with the thumbprint terrain scattered throughout the northern plains of Mars (Lockwood and Kargel, 1994). The volume of water from that source had to fill the basin above 200 m from the floor level to the -2350 m contour in order to discharge through the eastern outlet channel, following the braiding paths atop the volcanic terrain (Figure 5A). The connected channels suggest a distributed source, otherwise they would require multiple subsurface breakouts that would then follow separate paths. If a breakout resulted in significant discharge, it would likely concentrate in a single deep channel along the strongest topographic gradient or most mechanically susceptible rock layers. In contrast, the observed shallow, narrow channels are more consistent with minor

flow volumes sourced from a wider area with regional precipitation, likely a snow or ice layer. Channels fed by percipitation have an average bifurcation angle of 45° compared to groundwater sapping which has much wider bifurcation angles of 73° on average (Seybold et al., 2018). The low branching angle of 43° ± 21° indicates these channels were fed by precipitation.

4.2. Question 2. What terminated a large volcanic flow to preserve an isolated basin?

Question 2 arises given proximity to the Syrtis volcano with widespread and low viscosity lava flows (Bandfield et al., 2000; Ehlmann & Mustard, 2012; Simpson et al., 1982) that end abruptly at the basin margin after forming a topographically flat mesa. The basin had to survive regional volcanism, erosion of the surrounding terrains, and potential lacustrine fill to remain a topographic low. The 1100 km to the direct south of this small basin has been filled by Syrtis lava flows, so how did this depression persist despite similarly expected lava flow extent? The relatively flat nature of the rest of the Syrtis flows suggests low viscosity lavas that should have overflowed and filled the basin if they had encountered the modern landscape. We find the lava flows that were halted to be 1.3 Ga older than the ones that eventually infilled the basin. This suggests an obstruction that halted the volcanic flows near the irregular surface (Figure 5E), but disappeared subsequently to allow younger lava flows to infill the basin. The Syrtis Major volcanic flows range from 25 to 30 m (Hiesinger and Head, 2004), however, the cliffs formed at the flow terminations at the mesa are over 100 m. While the lava should have continued to flow based on the critical thickness estimates being much lower than the cliff heights, we also find the volcanic mesa to be many meters thicker than expected while also not following the local topography. This suggests the flows came in contact with an obstruction and caused a pooling effect at the base of the flows (Figure 11A) which would create both the topographically flat area, as well as the much thicker section of volcanics.

A higher Noachian plain could have stopped abutting lava flows, and eroded subsequently to the modern basin. However, it would be mechanically unlikely for aeolian or fluvial erosion to create the basin. Such processes can deflate surfaces or cut channels, but they commonly fill basins, not create them. Nevertheless, a depression could form through erosional processes if there was an initial heterogeneity in the Noachian material with spatially coincidental less-resistant material deflating to form the basin. That hypothesis is not testable with current satellite observations, due to resolution limits and difficulties in quantifying variations in relative ages. Alternatively, a friable, yet non-lithic material may have occupied the basin at the time of the lava flows. A simple mechanism that would fit the observations would be a >1 km thick ice sheet (Figure 11A). This would have halted lava flows (Figure 11A), and contributed the edge effects observed by Ivanov & Head (2003) that differ from volcanic flow terminations found elsewhere around Syrtis Major. Using numerical modeling, the proposed ice sheet thickness would range from around 1-2 km within this area, in line with our estimates based on the halting of the lava flows (Souček et al., 2015). The relatively thin ice sheet required for the hypothesis, compared to adjacent areas reaching thickness as high as 5 km (Souček et al., 2015), further enhances its feasibility.

4.3. Question 3. What enabled basin drainage via topographically higher outlet channels, despite the existence of a topographically lower potential outlet to the SE?

Question 3 reflects the divergence between the current landscape and the topographic contour lines that enclose the basin. Any lake level above the -2450 m contour that completely encloses the current basin would cause basin discharge through southeast passage. However, the eastern outlet channel has a head elevation of -2330 m, requiring an additional 120 m of water depth. The basin shows evidence for lacustrine deposition through the equipotential filling of the magnesium carbonate layer (Figure 8), in addition to the layered sulfate deposits along the outer edges of the basin with dip angles lower than 10° discussed in detail by Quinn & Ehlmann (2019).

We consider three hypotheses to explain the paradox of a developed eastern outlet channel despite the gravitationally favored drainage to the southeast.

The first hypothesis to explain the existence of the eastern outlet channel is that the current landscape may not represent the topography during the time of fluvial activity. Regional or local subsidence, uplift, or rebound, possibly from an ice sheet, could have modified the local topography enough to affect the boundaries of the paleolake shore and made the southeastern gap the low point in the basin rim, instead of the eastern outlet. However, this had to happen after the emplacement of the volcanics, the time of activity for this system, and would be expected to cause significant fracturing and faulting which are not observed.

A second hypothesis to explain the existence of the eastern outlet, is that a continuation of the sulfate and volcanic cap unit observed to the west of the passage may have created a barrier and blocked the southeastern passage. We do not observe significant fluvial erosion within this passage, although it may be obscured by the lag deposits and debris that floors the passage. However, fluvial morphology is absent even beyond the roughly ~ 3 km passage length obscured by such debris. Alternatively, landslides of sulfate and volcanic wall material could have formed a dam, followed by aeolian deflation after the fluvial activity ended, or by dam collapse during a late fluvial episode. However, given the absence of significant block, boulders, or breccia within the outlet and the surrounding area, the hypothesis of a lithic blockage is unsupported.

The third hypothesis for the existence of the eastern outlet is that ice-dams temporarily blocked flow though the southeast outlet. A ~40 degree obliquity occurring as recently as 5 Ma ago suggests the likelihood of glaciation at that time (Laskar et al., 2004). A mere 200 m high ice dam could block the southeast passage and force discharge through the eastern passage (Figure 11B). Regional ice units, of atmospheric provenance, would also be consistent with the evidence

for a diffuse source for the fluvial activity. The ablation of the ice dam after the basin drained, evaporated, or sublimated could remove evidence of the passage blockage without leaving traces of material (Figure 11B). The observed lack of fractures and faults, lack of a debris field, and lack of erosional features in the southeast passage would best be explained by the sublimated ice dam hypothesis.

4.4. Global Ocean Implications

In section 3.4 we mentioned a dissected fan that was potentially once a terminal delta at -3050 m. The relatively small and simple morphology suggests a short period of formation, or extensive resurfacing and erosion. The eroded nature of the fan precludes observations of deltaic structures such as topsets, foresets, and bottomsets and cannot uniquely distinguish between a dry alluvial fan emplacement and a submerged delta that underwent extensive erosion. The existence of additional channels down slope towards the Isidis Basin suggest multiple channel flow episodes occurring before the fan development so as not to be cut by the topographically lower channels. The channels may have once linked to the main system and might be remnants of an older, larger flow or a lower water level within Isidis. Alternatively, the channels may be independent of our system given their distance from the fan in conjunction with being separated by basin floor material.

The fan's topographic high of -3050 m approximates that of the delta located in the south of the Isidis Basin (Erkeling et al., 2012). However, the fan is located 250 m lower than the cliff forming shoreline in southern Isidis proposed by Erkeling et al., (2012) at -2800 m and 550 m lower than the shoreline proposed by Di Achille & Hynek, (2010) at -2500 m. While a global ocean is still a possibility, the existence of an ocean would not support morphology seen in this

area such as the irregular volcanic flow terminations, the preservation of this basin, and the outlet channels flowing to a topographically higher outlet than available.

4.5. Glacial Implications

Large scale glaciation has been suggested in the Northeast Syrtis region previously (Bramble et al., 2017; Guidat et al., 2015; Ivanov, 2003; Souček et al., 2015), which we advance with geomorphological observations revealing the possibility and extent of local ice deposits. To preserve the basin at the edge of the Syrtis Major flows, ice would need to have been present during the end stages of the Syrtis Major emplacement (Figure 11A), crater-counted to 3.4 Ga. Furthermore, while it is difficult to morphologically bound the height of ice, the basin is surrounded by coherent volcanic surfaces directly to the south that are 700 m higher than the deepest part of the basin and nearly 1000 m higher to the west where source channels are present. If the Syrtis Major lava or pyroclastic flows overtopped the ice unit, a visible volcanic debris field would be expected as the ice melted away. The lack of the volcanic debris field suggests that the ice sheet would have been at least 1 km thick when the current flow front formed, also consistent with numerical models which put the thickness of the potential ice sheet above this limit (Souček et al., 2015).

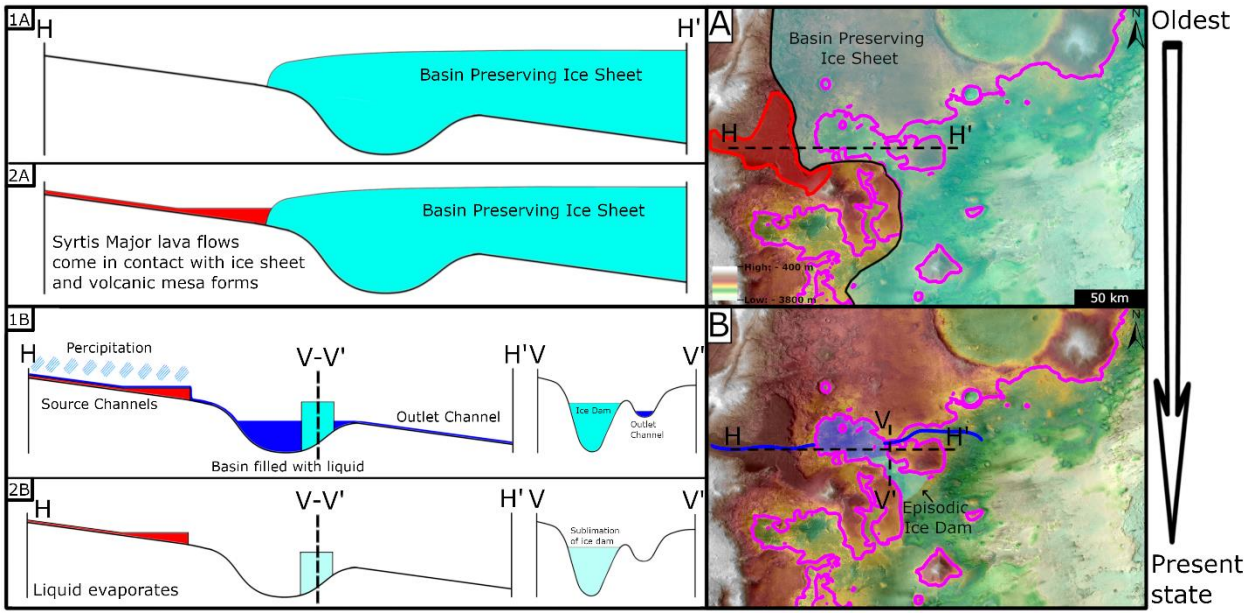

Figure 11. Timeline for the Northeast Syrtis area using generalized schematics. 1A and 2A correspond to ice position A. 1B and 2B correspond to ice position B.

Following the emplacement of the Syrtis Major volcanic flows the observed fluvial geomorphology and multiple outflow channels suggest multiple episodes of drainage based upon the multiple paths taken by the channels. That is consistent with climate cycles that episodically emplace regional ice with some basal melting. The outlet channels are too small and do not retain craters for accurate chronology. Higher resolution data would be needed to better resolve the number, duration, and possibly order of glacial episodes in their relation to the outlet channels. However, the most complex portion of the outlet channels show three parallel sections (Figure 7). If each drainage episode created a separate channel section, and a final episode drained through the modern southeastern break in the basin, a minimum of four discharge events are feasible. It is likely that channels sustained multiple, temporally separated, flows and that evidence of early events would have been eroded by later ones. This leaves open the possibility of a multitude of fluvial episodes that mirror climate cycles.

CONCLUSIONS

The Hesperian-aged fluvial system located on the northeast Syrtis boundary records important late stage geologic events that are vital to understanding the geologic history of the region. That system represents a second distinct episode of fluvial activity in the region, following the first associated with the Jezero open basin crater lake at 3.74 Ga (Fassett and Head, 2008). Our observations establish that this second episode occurred after the early Hesperian emplacement of Syrtis Major volcanics. The fluvial system is defined by high elevation upland source channels on the western basalts (Bandfield et al., 2000) that indicate the system's source, a topographic basin that indicates fluvial storage, and an outlet channel flowing toward the low elevation Isidis Basin. The diffuse source morphology and low branching angles suggest an atmospheric origin of the system's water. The basin is preserved at the base of Syrtis Major with low viscosity lava rheology that terminates in high cliffs suggesting they encountered a large ice sheet that was at least 1 km thick. The well-developed outlet channel is gravitationally disfavored and would require either significant obliteration of flow features on the southeast edge of the basin or a temporary paleo ice dam preventing such discharge, further constraining the geologic history of the region. Collectively, the observations contribute to a more detailed understanding of the late-stage glaciofluvial processes in the northeast Syrtis region,

Table 1. Targets, image IDs, instruments, and associated figures for each image used.

Target	Image ID	Instrument	Figure
Study Area Mosaic	E72_N16	CTX	2, 4, 5
Study Area Mosaic	E76_N16	CTX	2, 4, 5, 6, 7, 8, 10, 11
Proposed Fan	ESP_036407_1975_RED	HiRISE	9A, 9B
Sagan Crater Fan	B21_018003_1916_XN_11N030W	CTX	9C
Libya Montes Fan	D05_029260_1828_XN_02N274W.tiff	CTX	9D
Basin CRISM	FRT000199C7	CRISM	8C
Basin HiRISE	ESP_04882_1980_RED	HiRISE	8A, 8B

REFERENCES

Andrews-Hanna, J.C., Phillips, R.J., Zuber, M.T., 2007. Meridiani Planum and the global hydrology of Mars. Nature 446, 163–166. https://doi.org/10.1038/nature05594

Bandfield, J.L., Hamilton, V.E., Christensen, P.R., 2000. A global view of martian surface compositions from MGS-TES. Science (80-.). 287, 1626–1630. https://doi.org/10.1126/science.287.5458.1626

Bibring, J.P., Langevin, Y., Mustard, J.F., Poulet, F., Arvidson, Raymond, Gendrin, A., Gondet, B., Mangold, N., Pinet, P., Forget, F., Berthe, M., Gomez, C., Jouglet, D., Soufflot, A., Vincendon, M., Combes, M., Drossart, P., Encrenaz, T., Fouchet, T., Merchiorri, R., Belluci, G.C., Altieri, F., Formisano, V., Capaccioni, F., Cerroni, P., Coradini, A., Fonti, S., Korablev, O., Kottsov, V., Ignatiev, N., Moroz, V., Titov, D., Zasova, L., Loiseau, D., Pinet, Patrick, Douté, S., Schmitt, B., Sotin, C., Hauber, E., Hoffmann, H., Jaumann, R., Keller, U., Arvidson, Ray, Duxbury, T., Forget, François, Neukum, G., 2006. Global mineralogical and aqueous Mars history derived from OMEGA/Mars express data. Science (80-.). 312, 400–404. https://doi.org/10.1126/science.1122659

Bramble, M.S., Mustard, J.F., Salvatore, M.R., 2017. The geological history of Northeast Syrtis Major, Mars. Icarus 293, 66–93. https://doi.org/10.1016/j.icarus.2017.03.030

Crown, D.A., Ramsey, M.S., 2017. Morphologic and thermophysical characteristics of lava flows southwest of Arsia Mons, Mars. J. Volcanol. Geotherm. Res. 342, 13–28. https://doi.org/10.1016/j.jvolgeores.2016.07.008

Davila, A.F., Fairén, A.G., Stokes, C.R., Platz, T., Rodriguez, A.P., Lacelle, D., Dohm, J., Pollard, W., 2013. Evidence for Hesperian glaciation along the Martian dichotomy boundary. Geology 41, 755–758. https://doi.org/10.1130/G34201.1

Di Achille, G., Hynek, B.M., 2010. Ancient ocean on Mars supported by global distribution of deltas and valleys. Nat. Geosci. 3, 459–463. https://doi.org/10.1038/ngeo891

Dickson, J.L., Kerber, L., Fassett, C.I., Ehlmann, B.L., 2018. A global, blended CTX mosaic of Mars with vecotrized seam mapping: a new mosaicking pipeline using principles of non-destructive image editing., in: 49th Lunar and Planetary Science Conference 2018. https://doi.org/10.1590/s1809-98232013000400007

Edwards, B.R., Karson, J., Wysocki, R., Lev, E., Bindeman, I., Kueppers, U., 2013. Insights on lava-ice/snow interactions from large-scale basaltic melt experiments. Geology 41, 851–854. https://doi.org/10.1130/G34305.1

Edwards, L., Broxton, M., 2012. Automated 3D Surface Reconstruction from Orbital Imagery. Lunar Planet. Sci. Conf. (Vol. 39) 01461, 2419. https://doi.org/10.2514/6.2006-7435

Ehlmann, B.L., Mustard, J.F., 2012. An in-situ record of major environmental transitions on early Mars at Northeast Syrtis Major. Geophys. Res. Lett. 39. https://doi.org/10.1029/2012GL051594

Ehlmann, B.L., Mustard, J.F., Fassett, C.I., Schon, S.C., Head, J.W., Des Marais, D.J., Grant, J.A., Murchie, S.L., 2008a. Clay minerals in delta deposits and organic preservation potential on Mars. Nat. Geosci. 1, 355–358. https://doi.org/10.1038/ngeo207

Ehlmann, B.L., Mustard, J.F., Murchie, S.L., Poulet, F., Bishop, J.L., Brown, A.J., Calvin, W.M., Clark, R.N., Marais, D.J. Des, Milliken, R.E., Roach, L.H., Roush, T.L., Swayze, G.A., Wray, J.J., 2008b. Orbital Identification of Carbonate-Bearing Rocks on Mars. Science (80-.). 322, 1828–1832. https://doi.org/10.1126/science.1164759

Ehlmann, B.L., Mustard, J.F., Swayze, G.A., Clark, R.N., Bishop, J.L., Poulet, F., Des Marais, D.J., Roach, L.H., Milliken, R.E., Wray, J.J., Barnouin-Jha, O., Murchie, S.L., 2009. Identification of hydrated silicate minerals on Mars using MRO-CRISM: Geologic context near Nili Fossae and implications for aqueous alteration. J. Geophys. Res. E Planets 114. https://doi.org/10.1029/2009JE003339

Erkeling, G., Reiss, D., Hiesinger, H., Poulet, F., Carter, J., Ivanov, M.A., Hauber, E., Jaumann, R., 2012. Valleys, paleolakes and possible shorelines at the Libya Montes/Isidis boundary: Implications for the hydrologic evolution of Mars. Icarus 219, 393–413. https://doi.org/10.1016/j.icarus.2012.03.012

Fassett, C.I., Head, J.W., 2008. The timing of martian valley network activity: Constraints from buffered crater counting. Icarus 195, 61–89. https://doi.org/10.1016/j.icarus.2007.12.009

Fassett, C.I., Head, J.W., 2005. Fluvial sedimentary deposits on Mars: Ancient deltas in a crater lake in the Nili Fossae region. Geophys. Res. Lett. 32, 1–5. https://doi.org/10.1029/2005GL023456

Goudge, T.A., Mustard, J.F., Head, J.W., Fassett, C.I., 2012. Constraints on the history of open-basin lakes on Mars from the composition and timing of volcanic resurfacing. J. Geophys. Res. E Planets 117. https://doi.org/10.1029/2012JE004115

Goudge, T.A., Mustard, J.F., Head, J.W., Fassett, C.I., Wiseman, S.M., 2015. Assessing the mineralogy of the watershed and fan deposits of the Jezero crater paleolake system, Mars. J. Geophys. Res. Planets 120, 775–808. https://doi.org/10.1002/2014JE004782

Guidat, T., Pochat, S., Bourgeois, O., Souček, O., 2015. Landform assemblage in Isidis Planitia, Mars: Evidence for a 3 Ga old polythermal ice sheet. Earth Planet. Sci. Lett. 411, 253–267. https://doi.org/10.1016/j.epsl.2014.12.002

Hartmann, W.K., 2005. Martian cratering 8: Isochron refinement and the chronology of Mars. Icarus 174, 294–320. https://doi.org/10.1016/j.icarus.2004.11.023

Hiesinger, H., Head, J.W., 2004. The Syrtis Major volcanic province, Mars: Synthesis from Mars Global Surveyor data. J. Geophys. Res. 109. https://doi.org/10.1029/2003je002143

Hirt, C., Claessens, S.J., Kuhn, M., Featherstone, W.E., 2012. Kilometer-resolution gravity field of Mars: MGM2011. Planet. Space Sci. 67, 147–154. https://doi.org/10.1016/j.pss.2012.02.006

Ivanov, M.A., 2003. Syrtis Major and Isidis Basin contact: Morphological and topographic characteristics of Syrtis Major lava flows and material of the Vastitas Borealis Formation. J. Geophys. Res. 108, 5063. https://doi.org/10.1029/2002je001994

Laskar, J., Correia, A.C.M., Gastineau, M., Joutel, F., Levrard, B., Robutel, P., 2004. Long term evolution and chaotic diffusion of the insolation quantities of Mars. Icarus 170, 343–364. https://doi.org/10.1016/j.icarus.2004.04.005

Lockwood, J., Kargel, J., 1994. Thumbprint Terrain in Isidis Planitia: Formed in a Glacial Paleolake Environment, in: Lunar and Planetary Institute Science …. p. 799.

Malin, M.C., Bell, J.F., Cantor, B.A., Caplinger, M.A., Calvin, W.M., Clancy, R.T., Edgett, K.S., Edwards, L., Haberle, R.M., James, P.B., Lee, S.W., Ravine, M.A., Thomas, P.C., Wolff, M.J., 2007. Context Camera Investigation on board the Mars Reconnaissance Orbiter. J. Geophys. Res. E Planets 112. https://doi.org/10.1029/2006JE002808

Mangold, N., Ansan, V., Baratoux, D., Costard, F., Dupeyrat, L., Hiesinger, H., Masson, P., Neukum, G., Pinet, P., 2008. Identification of a new outflow channel on Mars in Syrtis Major Planum using HRSC/MEx data. Planet. Space Sci. 56, 1030–1042. https://doi.org/10.1016/j.pss.2008.01.011

McEwen, A.S., Eliason, E.M., Bergstrom, J.W., Bridges, N.T., Hansen, C.J., Delamere, W.A., Grant, J.A., Gulick, V.C., Herkenhoff, K.E., Keszthelyi, L., kirk, R.L., Mellon, M.T., Squyres, S.W., Thomas, N., Weitz, C.M., 2007. Mars reconnaissance orbiter's high resolution imaging science experiment (HiRISE). J. Geophys. Res. E Planets 112. https://doi.org/10.1029/2005JE002605

McEwen, A.S., Preblich, B.S., Turtle, E.P., Artemieva, N.A., Golombek, M.P., Hurst, M., Kirk, R.L., Burr, D.M., Christensen, P.R., 2005. The rayed crater Zunil and interpretations of small impact craters on Mars. Icarus 176, 351–381. https://doi.org/10.1016/j.icarus.2005.02.009

McGuire, P.C., Bishop, J.L., Brown, A.J., Fraeman, A.A., Marzo, G.A., Frank Morgan, M., Murchie, S.L., Mustard, J.F., Parente, M., Pelkey, S.M., Roush, T.L., Seelos, F.P., Smith, M.D., Wendt, L., Wolff, M.J., 2009. An improvement to the volcano-scan algorithm for atmospheric correction of CRISM and OMEGA spectral data. Planet. Space Sci. 57, 809–815. https://doi.org/10.1016/j.pss.2009.03.007

Murchie, S., Arvidson, R., Bedini, P., Beisser, K., Bibring, J.P., Bishop, J., Boldt, J., Cavender, P., Choo, T., Clancy, R.T., Darlington, E.H., Des Marais, D., Espiritu, R., Fort, D., Green, R., Guinness, E., Hayes, J., Hash, C., Heffernan, K., Hemmler, J., Heyler, G., Humm, D., Hutcheson, J., Izenberg, N., Lee, R., Lees, J., Lohr, D., Malaret, E., Martin, T., McGovern, J.A., McGuire, P., Morris, R., Mustard, J., Pelkey, S., Rhodes, E., Robinson, M., Roush, T., Schaefer, E., Seagrave, G., Seelos, F., Silverglate, P., Slavney, S., Smith, M., Shyong, W.J., Strohbehn, K., Taylor, H., Thompson, P., Tossman, B., Wirzburger, M., Wolff, M., 2007. Compact Connaissance Imaging Spectrometer for Mars (CRISM) on Mars Reconnaissance Orbiter (MRO). J. Geophys. Res. E Planets 112. https://doi.org/10.1029/2006JE002682

Mustard, J.F., Cooper, C.D., Rifkin, M.K., 2001. Evidence for recent climate change on Mars from the identification of youthful near-surface ground ice. Nature 412, 411–414. https://doi.org/10.1038/35086515

Mustard, J.F., Ehlmann, B.L., Murchie, S.L., Poulet, F., Mangold, N., Head, J.W., Bibring, J.P., Roach, L.H., 2009. Composition, morphology, and stratigraphy of Noachian crust around the Isidis basin. J. Geophys. Res. E Planets 114. https://doi.org/10.1029/2009JE003349

Mustard, J.F., Poulet, F., Head, J.W., Mangold, N., Bibring, J.P., Pelkey, S.M., Fassett, C.I., Langevin, Y., Neukum, G., 2007. Mineralogy of the Nili Fossae region with OMEGA/Mars Express data: 1. Ancient impact melt in the Isidis Basin and implications for the transition from the Noachian to Hesperian. J. Geophys. Res. E Planets 112. https://doi.org/10.1029/2006JE002834

Neukum, G., Jaumann, R., 2004. HRSC: The high resolution stereo camera of Mars Express, in: Mars Express: The Scientific Payload. Mars Express Sci. payload. Ed. by Andrew Wilson 1–19.

Palumbo, A.M., Head, J.W., 2018. Impact cratering as a cause of climate change, surface alteration, and resurfacing during the early history of Mars. Meteorit. Planet. Sci. 53, 687–725. https://doi.org/10.1111/maps.13001

Quinn, D.P.P., Ehlmann, B.L.L., 2019. The deposition and alteration history of the northeast Syrtis layered sulfates. J. Geophys. Res. Planets. https://doi.org/10.1029/2018je005706

Rothery, D.A., McBride, N., Gilmour, I., 2003. An Introduction to the Solar System. Cambridge University Press.

Salese, F., Pondrelli, M., Neeseman, A., Schmidt, G., Ori, G.G., 2019. Geological Evidence of Planet-Wide Groundwater System on Mars. J. Geophys. Res. Planets. https://doi.org/10.1029/2018JE005802

Schaber, G.G., 2008. Syrtis major: A low-relief volcanic shield. J. Geophys. Res. 87, 9852. https://doi.org/10.1029/jb087ib12p09852

Schon, S.C., Head, J.W., Fassett, C.I., 2012. An overfilled lacustrine system and progradational delta in Jezero crater, Mars: Implications for Noachian climate. Planet. Space Sci. 67, 28–45. https://doi.org/10.1016/j.pss.2012.02.003

Seybold, H., Rothman, D.H., Kirchner, J.W., 2017. Climate's watermark in the geometry of stream networks. Geophys. Res. Lett. 44, 2272–2280. https://doi.org/10.1002/2016GL072089

Seybold, H.J., Kite, E., Kirchner, J.W., 2018. Branching geometry of valley networks on mars and earth and its implications for early martian climate. Sci. Adv. 4, 1–6. https://doi.org/10.1126/sciadv.aar6692

Simpson, R.A., Tyler, G.L., Harmon, J.K., Peterfreund, A.R., 1982. Radar measurement of small-scale surface texture: Syrtis major. Icarus 49, 258–283. https://doi.org/10.1016/0019-1035(82)90076-8

Souček, O., Bourgeois, O., Pochat, S., Guidat, T., 2015. A 3 Ga old polythermal ice sheet in Isidis Planitia, Mars: Dynamics and thermal regime inferred from numerical modeling. Earth Planet. Sci. Lett. 426, 176–190. https://doi.org/10.1016/j.epsl.2015.06.038

Stolper, E., Walker, D., 1980. Melt density and the average composition of basalt. Contrib. to Mineral. Petrol. 74, 7–12. https://doi.org/10.1007/BF00375484

Susko, D., Karunatillake, S., Kodikara, G., Skok, J.R., Wray, J., Heldmann, J., Cousin, A., Judice, T., 2017. A record of igneous evolution in Elysium, a major martian volcanic province. Sci. Rep. 7, 43177. https://doi.org/10.1038/srep43177

Tornabene, L.L., Moersch, J.E., McSween, H.Y., Hamilton, V.E., Piatek, J.L., Christensen, P.R., 2008. Surface and crater-exposed lithologic units of the Isidis based as mapped by coanalysis of THEMIS and TES derived data products. J. Geophys. Res. E Planets 113. https://doi.org/10.1029/2007JE002988

Werner, S.C., 2008. The early martian evolution-Constraints from basin formation ages. Icarus 195, 45–60. https://doi.org/10.1016/j.icarus.2007.12.008

Wichman, R.W., Schultz, P.H., 2008. Sequence and mechanisms of deformation around the Hellas and Isidis Impact Basins on Mars. J. Geophys. Res. 94, 17333. https://doi.org/10.1029/jb094ib12p17333

Wilson, L., Head, J.W., 1994. Review and analysis of volcanic eruption to theory relationships landforms. Rev. Geophys. 32, 221–263.

Zuber, M.T., 1992. The Mars Observer laser altimeter investigation. J. Geophys. Res. 97, 7781–7797. https://doi.org/10.1029/92JE00341

VITA

Connor Matherne began his academic venture initially as a petroleum engineer, before discovering his love for geology and all things rocks. He focuses his research on morphological characteristics within geology on both Earth and Mars. On Earth, most of his work revolves around laboratory analysis of samples and thin sections. While on Mars, his research looks at morphology associated with Early Mars climate evolution. During his free time, Matherne is a renowned astrophotographer, with many of his photographs ending up in books, magazines, articles online, museums, and accumulating millions of views across multiple countries. Matherne plans to graduate in December of 2019.